Repositorio Institucional de la Universidad Autónoma de Madrid

Incorporation of Photocatalytic Pt(II) Complexes into Imine-Based Layered Covalent Organic Frameworks (COFs) through Monomer Truncation Strategy

Alberto López-Magano,[a] Ana E. Platero-Prats,[a,b] Silvia Cabrera,[a,c]* Rubén Mas-Ballesté[a,c]* and Jose Alemán[c,d]*

a.   Inorganic Chemistry Department, Módulo 7, Universidad Autónoma de Madrid, 28049 Madrid, Spain.

b.   Condensed Matter Physics Center (IFIMAC), Universidad Autónoma de Madrid, Campus de Cantoblanco, 28049 Madrid, Spain

c.   Institute for Advanced Research in Chemical Sciences (IAdChem), Universidad Autónoma de Madrid, 28049 Madrid, Spain.

d.   Organic Chemistry Department, Módulo 1, Universidad Autónoma de Madrid, 28049 Madrid, Spain.

E-mail: ruben.mas@uam.es, jose.aleman@uam.es

Abstract

A new photoactive Pt (II) hydroxyquinoline complex has been covalently linked into the structure of an imine-based layered covalent organic framework (COF) through the monomer truncation strategy. Such strategy allows the incorporation of molecular fragments with only one functional group able to condensate into the imine-framework. The photocatalytic activity of the resulting Pt@COF has been applied to the oxidation of sulfides to sulfoxides, obtaining excellent results for all the studied cases, and showing that in this reaction goes through both photoredox and energy transfer processes. The results obtained showed a great enhancement of the catalytic activity (up to 25000 turnover number, TON), stability and a significant decrease on the reaction times, as a consequence of immobilization and isolation of Pt(II) centers into the organic framework. In addition, Pt@COF has been proved to be an excellent heterogeneous photocatalyst also in exclusive photoredox processes, reaching 7500 TON in hydrodebromination reactions.

Keywords: Covalent Organic Frameworks, COF, Photochemistry, Platinum, Photoredox.

1. Introduction

Since their discovery in 2005,[1] covalent organic frameworks have been established as a new type of very promising organic porous materials with interesting applications such as gas storage,[2–4] energy storage,[5–10] drug delivery,[11] proton conduction, [12–15] optoelectronics [16–18] and catalysis.[19–22] The possibility of tuning the COF structure and pore size, depending on the different building blocks of which they are composed, provides an enormous versatility.

In the catalysis field, a variety of contributions can be found using COFs as catalytic materials as a result of incorporation of metal species.[19,23,24] For this area,

the main approach consists on the design of typical ligands modified in such a way that can act as building blocks for the construction of the COF. Such typical ligands (Salen,[25] catechol,[26] bipyridine,[27] and porphyrin-based[28] building blocks) are able to coordinate a variety of metals. Different divalent metals such as Co and Zn introduced into Salen-based COFs were used in Henry-type reactions.[25] In addition, Vanadium centres have been coordinated to catechol-derivatives inserted in a COF backbone, presenting high activity in oxidation and Prins reactions.[26] Moreover, Pd and Mn were attached to bipyridine moieties and were used in Heck-epoxidation tandem reactions.[27] Finally, porphyrin-based COFs were successfully isolated with a variety of metal centres. For example, Fe-porphyrin-based COFs were used to decompose hydrogen peroxide, and also in the obtention of highly ordered pyrolytic graphite.[29] Nevertheless, all the examples presented above require the challenging design of ligands as building blocks that contain two, three or four functional groups in the appropriate symmetry, able to condensate into the COF structure. This requirement directly affects the final structure of the COF and usually implies difficult syntheses. It would be easier to have a unique functional group to be attached to the COF structure, requiring, in general, less synthetic steps.

Very recently, an interesting strategy for the incorporation of molecular fragments into a COF structure has been described. [30–33] This approach, named as monomer truncation strategy, consists of blocking one of the linking points of a building block. In such a way, this blocking generates structural defects, which are randomly distributed into the COF backbone. On one hand, it has been employed for the functionalization of both 3D and 2D boronate-based COFs, in order to modulate the crystal growth process. On the other hand, such strategy has been used for the incorporation of fragments useful for the attachment of fluorescent organic dyes through post-functionalization.[32]

Nevertheless, the application of the monomer truncation strategy has never been studied on metal-based catalytic systems and photocatalytic systems.

In this work, we present, to the best of our knowledge, an unreported strategy to isolate and immobilize catalytic metal complexes into the structure of an imine-based layered COF through monomer truncation. In particular, we choose Pt(II)-hydroxyquinoline fragment as a photoactive catalytic centre[34] in order to perform both energy transfer and photoredox processes. For this purpose, we incorporate an aldehyde group into the ligand, able to condensate as an imine into the COF backbone. The main advantage of this strategy is the use of metal complexes that contain only one functional group, instead of the generally required two, three or four functionalities in predetermined symmetries. Therefore, using this strategy, the difficulty of the synthesis of molecular precursors is significantly decreased. Aiming to evaluate the advantages of introducing such Pt centers into COF backbones, we compare the inherent photocatalytic activity of both molecular Pt complex and undecorated imine-based COFs,[35] with that of the new hybrid material. Catalytic activity of the **Pt@COF** will be first studied in the photooxidation of sulfides via energy transfer, whereas photoredox processes are expanded through photohydrodebromination reactions [36], showing the great photocatalytic potential of this new truncate strategy in materials.

2. Experimental.

2.1. Materials and methods.

All reagents and solvents were purchased from commercial sources and used without further purification.

Light irradiation was carried out using a 15W blue LED photoreactor thermostated at 25 ˚C. A spectro-radiometer equipment *Stellarnet* model *Blue-Wave UV-NB50* was employed

to measure the emission of the Blue LED used (range 300-600 Λ, integration time CR2-AP + 200 ms, intensity 21.7217 W/m^2).

Nuclear Magnetic Resonance (NMR) spectra were acquired on a *Bruker AV-300 spectrometer*, running at 300 MHz for ^1H, at 75 MHz for ^{13}C and at 65.5 Hz for ^{195}Pt. ^{13}C solid State Nuclear Magnetic Resonance were acquired on a *Bruker AV-400 spectrometer* coupled to a multinuclear probe (^{15}N-^{31}P) CPMAS with triple channel (BL4 X/Y/^1H) for a 4 mm rotor at room temperature, using 1k scans and 12 kHz of turning speed. The ^1H excitation pulse used is $\pi/2 * 2.75$ μs and the contact pulse is 3 ms.

Powder X-ray difraction was obtained in a *X'Pert PRO* difractometer $\theta/2\theta$ geometry from *Panalytica*l equipped with a *Johansson* monochromator for Λ K_α, a *X'Celerator* fast detector in an alumina holder. The $\theta/2\theta$ swept was performed from 4 to 45 ° with an angular increase of 0.0167 °/100 s.

Scanning Electron Microscopy (SEM) images were carried out on a *Hitachi S-3000N electron microscope* with a coupled ESED detector and an analyzer from energy dispersive X-ray from *Oxford Instruments*, *INCAx-sight* model. The images were obtained in vacuum after being metallized in a *Sputter Quórum Q150T-S* with gold coating.

Qualitative and quantitative Total X-Ray Fluorescence analyses (TXRF) were performed with a benchtop *S2 PicoFox* TXRF spectrometer from Bruker Nano (Germany) [37,38]. TXRF system was equipped with a Mo X-ray source working at 50 kV and 600 μA, a multilayer monochromator with 80% of reflectivity at 17.5 keV (Mo K_α), a XFlash SDD detector with an effective area of 30 mm^2 and an energy resolution better than 150 eV for 5.9 keV (Mn K_α). For deconvolution and integration commercial Spectra v. 7.5.3 software package from Bruker was used. Previously to the measurements, sample acid digestions were performed in a high pressure and temperature microwave. Acid digestion technology was used

by mean of an UltraWAVE digestion system from Millestone (Italy) with a single reaction chamber able of operates up to 199 bar pressure and 270 °C.

Synchrotron X-ray total scattering data suitable for Pair Distribution Function (PDF) analyses were collected at the P02.1 beamline at *PETRA IIII* using 60 keV (0.207 Å) X-rays. Samples were loaded into kapton capillaries and sealed using epoxy. Data were collected using an amorphous silicon-based *PerkinElmer* detector area detector. Geometric corrections and reduction to one-dimensional data used DAWN Science software.[39] PDFs were obtained from the data using PDFgetX3[40] within xPDFsuite software to a Q_{max} = 10 Å^{-1} and 17 Å^{-1}, for the solutions and the solids, respectively.

2.2. Experimental Procedures.

Synthesis of complex 2: The synthesis of complex **2** was performed following a previously reported procedure for similar Pt(II)-hydroxyquinoline complexes.[34] To a solution of NaOH (18 mg, 0.474 mmol) in MeOH (0.9 mL), **L2** (82 mg, 0.474 mmol) and acetone (1.8 mL) were added. To the brown suspension, *cis*-PtCl$_2$(dmso)$_2$ (200 mg, 0.474 mmol) was added. The mixture was stirred at room temperature and in the absence of light during 24 h. The complex was isolated by filtration, washed with water and Et$_2$O and dried at vacuum. Yellow solid, 210 mg obtained (92% Yield). ^{1}H-NMR (300 MHz, DMSO-d^6) δ 10.08 (s, 1H), 9.74 (d, J = 8.7 Hz, 1H), 9.43 (dd, J = 5.4, 1.1 Hz, 1H), 8.15 (dd, J = 8.4 Hz, 1H), 7.92 (dd, J = 8.6, 5.4 Hz, 1H), 7.10 (d, J = 8.3 Hz, 1H) ppm. ^{13}C-NMR (75 MHz, DMSO-d^6) δ 190.8, 172.4, 148.7, 143.8, 141.7, 137.4, 128.8, 125.1, 119.2, 113.6, 45.9 ppm. ^{195}Pt-NMR (64.5 MHz, DMSO-d^6) δ -2735.9 ppm. MS (ESI$^+$) m/e = 481 (M$^+$). Elemental analysis: calculated for C$_{12}$H$_{12}$ClNO$_3$PtS: C: 29.98%; H: 2.52%; N: 2.91%; S: 6.67%. Found: C: 30.01%; H: 2.56%; N: 2.95%; S: 6.45%.

Synthesis of Pt@COF: In a 50 mL two-necked round bottom flask equipped with an addition funnel, molecular sieves 3A and 1,3,5-tris(4-aminophenyl)benzene **TAPB** (103 mg,

0.293 mmol) were added. The system was purged with three vacuum-Ar cycles. Then, 5 mL of dry DMSO and 220 µL of glacial acetic acid were added. A solution of complex **2** (35 mg, 0.073 mmol) in 6 mL of dry DMSO was added dropwise using the addition funnel. Once this addition was completed, the mixture was stirred during 30 minutes at room temperature. This mixture was filtered under Ar and transferred via cannula to a 50 mL round bottom flask that contains 1,3,5-benzenetricarbaldehyde **BTCA** (48 mg, 0.293 mmol) dissolved in 5 mL of dry DMSO and 250 µL of glacial acetic acid. The reaction stirred during 24 h at room temperature. Then, it was isolated by filtration and washed with DMSO, MeOH and THF. The yellow solid was immersed in 7 mL of THF during 24 h, then filtered again and activated under vacuum and 80 ºC overnight. For the characterization, see Supporting Information.

Synthesis of Pt@COF-Annealed: The **Pt@COF-Annealed 1d** was synthesized following an adapted reported procedure.[41] A 45 mL solvothermal reactor was charged with **Pt@COF** (80 mg), 6.4 mL of a mixture of anhydrous dioxane : mesitylene (5:1), 1.3 mL of distilled water and 1.9 mL of glacial acetic acid. The reactor was heated at 120 ˚C for 3 days, yielding a yellow solid which was isolated by filtration and washed with toluene and THF. The resulting powder was immersed in anhydrous THF for 24 h and dried first at room temperature under vacuum for 12 h, and then at 100 ˚C for 2 h to afford a yellow powder, **Pt@COF-Annealed**.

General procedure for the photooxidation of sulfides: An oven-dried 10 mL vial equipped with a magnetic stir bar was charged with catalyst (2.4 mg) and the corresponding sulfide **3** (0.3 mmol). Then, 2 mL of MeOH were added. The vial was closed with a PTFE / rubber septum and the reaction mixture was degassed by three cycles vacuum / oxygen of "freeze-pump-thaw". Then the vial was placed on a blue light LED photoreactor (450 nm) with

an O_2 balloon and the reaction mixture was stirred at 25 ˚C. The reaction was monitored by TLC and ^{1}H-NMR. After the total consumption of the sulfide, the crude was filtered through membrane filter and purified by flash chromatography.

General procedure for the photohydrodebromination of organic bromides: An oven-dried 7 mL vial equipped with a magnetic stir bar was charged with catalyst (2.4 mg) and the corresponding bromoderivative (0.3 mmol). Then, 3 mL of EtOH were added. The vial was closed with a PTFE / rubber septum and the reaction mixture was degassed by three cycles vacuum / Argon of "freeze-pump-thaw". Then the vial was placed on a blue light LED rack (450 nm) with an Ar balloon and the reaction mixture was stirred at 25 ˚C. The reaction was monitored by TLC and ^{1}H-NMR. After the total consumption of the reactant, the crude was filtered and purified by flash chromatography.

3. Result and Discussion

### 3.1. Synthesis and characterization.

To accomplish the strategy presented in the introduction, we designed a Pt(II)-hydroxyquinoline complex bearing an aldehyde group, which should allow to covalently attach it to the organic framework. First, the synthesis of the ligand was made by a modification of a reported Reimer-Tiemann reaction.[42] Later, the complexation reaction was carried out according to a previously reported procedure.[34] Spectroscopic characterization of both ligand **L2** and complex **2** agreed well with the expected structures. Furthermore, complex **2** was characterized by single crystal X-ray diffraction,[43] confirming the predicted formulation (See Scheme 1 and Supporting Information for further details). In addition, for comparison purposes, we prepared complex **1**, as parent complex with photocatalytic activity, but that cannot be covalently

8

incorporated as a structural defect into the COF backbone, since it does not contain an

aldehyde group into its structure.
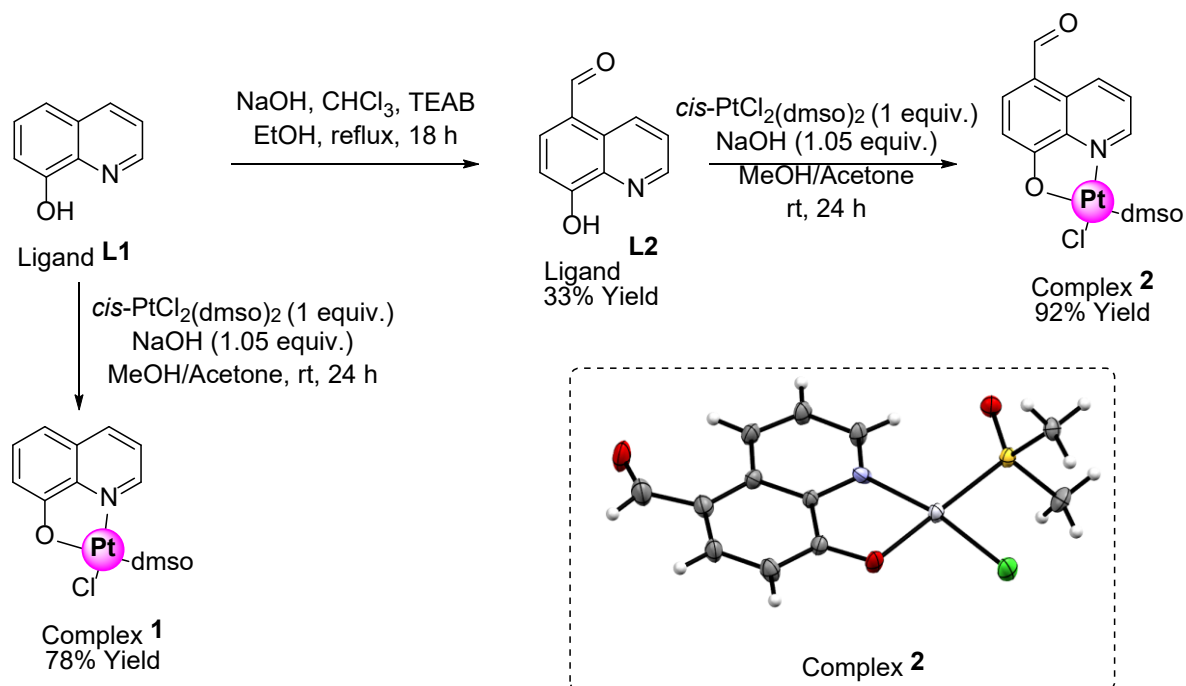
Scheme 1: Synthesis of complex **1** and **2**, and single crystal X-ray structure.

Once complex **2** was satisfactorily prepared, we proceeded to the synthesis of the

hybrid material. We chose a simple imine-based layered COF as a model platform,

formed by the **TAPB** and **BTCA** under mild acidic conditions (see Scheme 2).
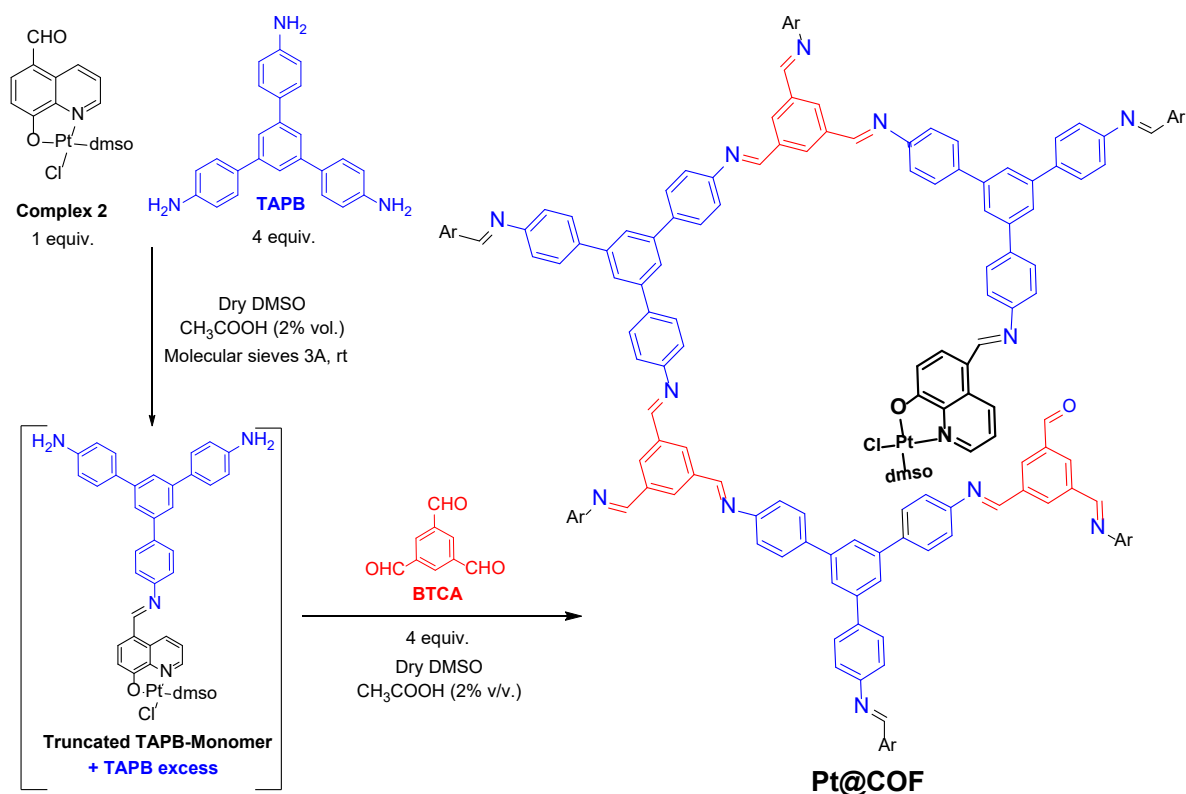
Scheme 2: Synthesis of Pt@COF under mild acidic conditions.

The first step of COF synthesis consisted in the incubation during 1 hour of the complex in the presence of an excess of the **TAPB** (1:4), using DMSO as solvent and acetic acid (2%) as catalyst. The truncated monomer is generated *in situ,* without isolation of the possible imine products. Then, the mixture was forced to react with a stoichiometric amount of **BTCA** in DMSO. After 24h of reaction, a yellow solid precipitated which was isolated by filtration. The obtained **Pt@COF** material was firstly characterized by Fourier-Transformed Infrared Spectroscopy (FTIR), observing the typical peaks for a polyimine layered COF (Figure 1d, black line): a) the imine C=N and C-C=N-C stretching bands, which appear at 1616 cm^{-1} and 1262 cm^{-1}, respectively, and b) the corresponding aromatic ring stretchings at 1590, 1500 and 1445 cm^{-1}. In addition, ^{13}C-NMR experiments using Cross Polarization combined to Magic Angle Spinning

(^{13}C-CP-MAS) were performed. The signal at 157 ppm (which corresponds to the iminic carbon) and the aromatic signals (148, 138, 128, 122 and 116 ppm) perfectly match with those observed in comparable pristine layered-COFs (see Supporting Information). [44] The Powder X-ray Diffraction (PXRD) pattern showed wide diffraction peaks, suggesting the formation of a material with moderated crystallinity. Thus, albeit with low intensities, the signals centred at 5.7 and 9.9 degrees can be clearly distinguished. According to simulated diffraction pattern previously reported (see Supporting Information) [45], such peaks correspond to the indexed planes (100) and (110), (Figure 1c), black line). A layered microstructure was observed by SEM images (Figure 1a). Total X-ray Fluorescence (TXRF) analysis were performed in order to determine the quantity of Pt incorporated into the COF structure, resulting on a 0.3% wt. Such low incorporation of complex could be attributed to the reversible nature of imine bonds that results in self-healing of structural defects, allowing only a limited extent of introduction of functional groups as defective sites in the covalent framework. Accordingly, similar results were obtained on synthesis using higher amounts of complex **2**. Interestingly, although such low loading represents a minimal structural deviation from pristine material, it has been proved to be catalytically relevant (see below). Specially, in photocatalytic processes, high catalytic loadings are not generally favourable due to the self-quenching of the excited states. Thus, considering both features, we did not further attempt higher Pt loadings.

In order to improve the crystallinity, the **Pt@COF** was subjected to solvothermal conditions (see Supporting Information), as previously reported for related COF systems. [41] Treatment at 120 ^{0}C of **Pt@COF** in a 1:5 mesitylene-dioxane mixture in presence of 10 M aqueous acetic acid resulted on a layered crystalline COF (**Pt@COF-Annealed**), that showed a significant improvement on the diffraction pattern by PXRD

11

(Figure 1c, red line). Layered microstructure was also confirmed by Scanning Electron Microscopy (SEM). The chemical identity of the COF was evaluated by FTIR and ^{13}C-CP-MAS-NMR, which is identical to that of the **Pt@COF**. Interestingly, thermal treatment did not imply leaching of platinum complex and therefore, the platinum content measured by TXRF was kept at 0.3% wt (see Supporting Information).
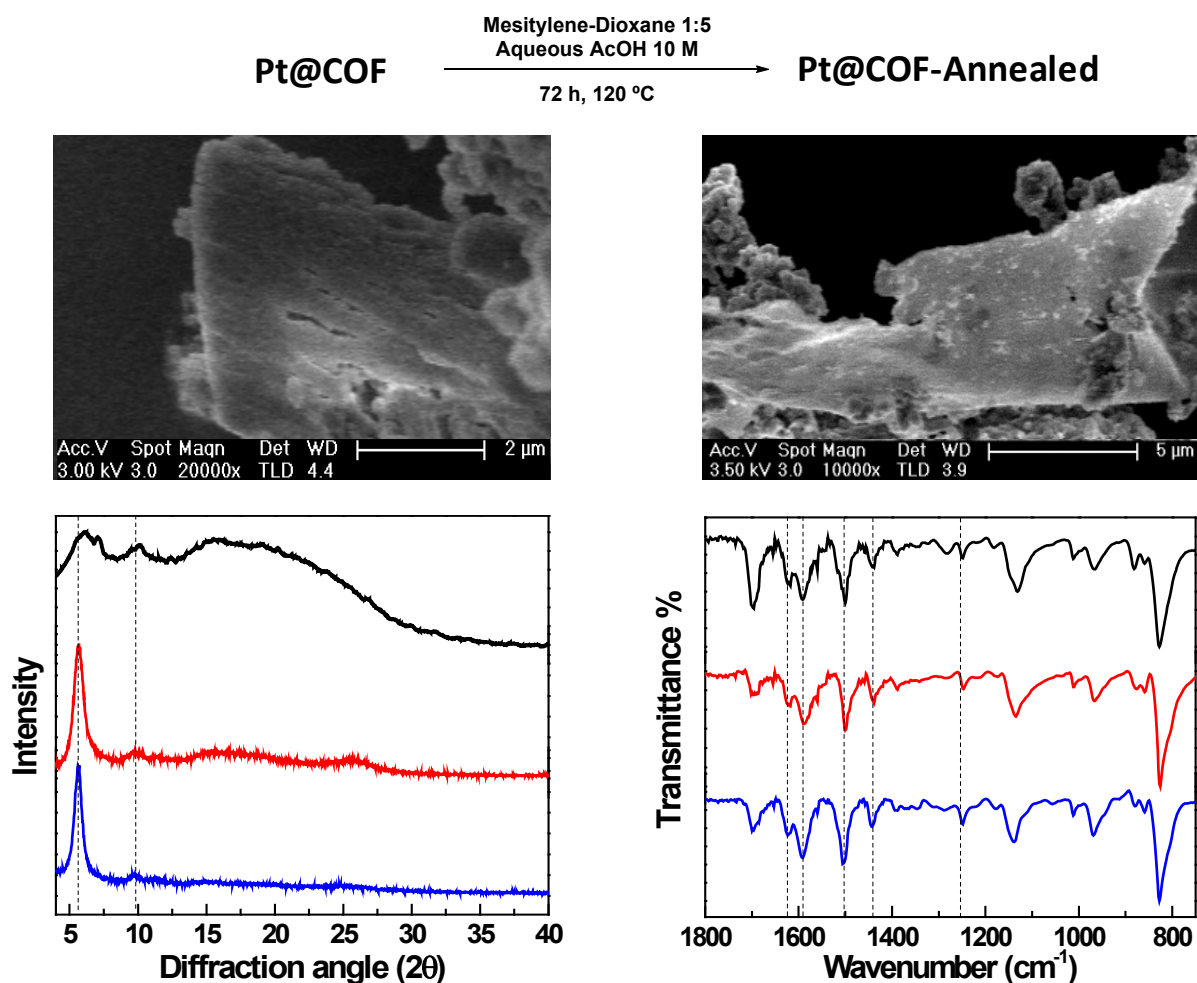

Figure 1: Characterization of **Pt@COF** and **Pt@COF-Annealed**. a) Scanning Electron Microscopy image of **Pt@COF**. b) Scanning Electron Microscopy image of **Pt@COF-Annealed**. c) Comparison of the PXRD patterns of **Pt@COF** (black), **Pt@COF-Annealed** (red) and **Pristine COF-Annealed** (blue). d) Comparison of the FTIR spectra of **Pt@COF** (black), **Pt@COF-Annealed** (red) and **Pristine COF-Annealed** (blue).

In order to understand the role of the aldehyde group in complex **2**, we decided to synthesize an analogous material using complex **1**, which do not contain the carbonyl fragment. In absence of a functional group that can condensate with amines, such compound should not be incorporated and only could maintain weak interactions with the COF. After material's synthesis, qualitative TXRF analysis did not shown detectable quantities of Pt (see Supporting Information). Therefore, carbonyl group is essential to charge the material with some amount of platinum complex and when it is incorporated, it is stable enough to not leak after at least 72 hours on suspension under high temperatures (see above). Such observations give evidence that platinum complex is covalently attached to the covalent organic framework as structural defects. To demonstrate such structural model, we performed Pair Distribution Function (PDF) analysis of synchrotron X-ray total scattering data. Such measurements allowed us to probe the local structure of the platinum centres within the COF. Differential PDF data (d-PDF), calculated by subtracting the signal of the pristine COF to that of **Pt@COF**, showed the occurrence of narrow correlations up to ~14 Å, demonstrating that the Pt complex is covalently bonded to the COF framework. Moreover, the contribution centred at ~2.32 Å is characteristic of Pt-Cl and Pt-S bond distances (Figure 2). Additionally, the broad d-PDF peak observed for **Pt@COF** also contains a subtle contribution around ca. 2.1 Å linked to Pt-N,O distances. Due to the low content of platinum complex on the **Pt@COF**, together with the strong X-ray scattering power of Cl and S, the d-PDF signal is shifted to the Pt-Cl,S bond distance values.
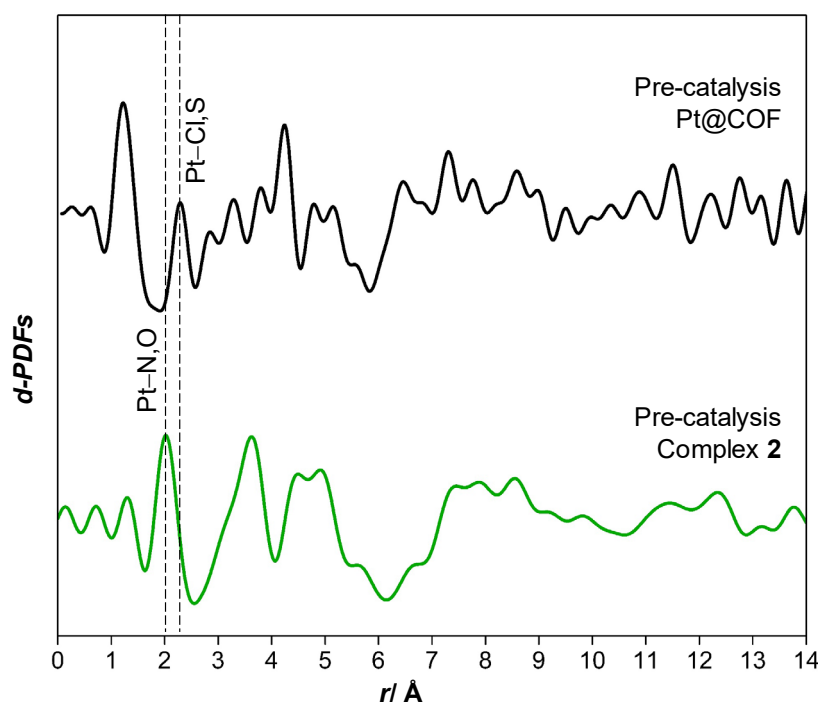
Figure 2: d-PDF data obtained for **Pt@COF** system as solid (black) in comparison with complex 2 in solution (green) before catalysis. The significant contribution at ~1.25 Å for **Pt@COF** is associated with the presence of guest organic molecules within the COF pores. For further details of the PDF analyses, see Supporting Information.

3.2. Photocatalytic activity: sulfoxidation reaction.

3.2.1. Screening of the catalyst. The catalytic performance of both **Pt@COF** and **Pt@COF-Annealed** were evaluated using as a model reaction the photosulfoxidation of the methyl(*p*-tolyl)sulfide (Table 1), which has been previously reported for complex **1** [34,46] and different COF-based systems.[47,48] As a control experiment, we evaluated the performance of the **pristines COF** and **COF-Annealed**. After 7 hours of reaction at room temperature irradiating at 450 nm in an O_2 saturated atmosphere, pristine COFs showed poor reaction conversions (10% and 33%, see Table 1, entries 4 and 5). Interestingly, for pristine materials, crystallinity (which is improved in pristine **COF-Annealed**) is a key factor to enhance the catalytic performance, which was

attributed to the beneficial effect of improving the extended conjugation across the material. In contrast, while **Pt@COF** accounts for 88% of conversion, under the same conditions **Pt@COF-Annealed** allows to obtain a conversion of 75%. These results suggest that the activity observed is mainly due to the isolated Pt centers instead of the overall material. Thus, as observed for other functionalized COFs, [49] while improved conjugation is not a decisive factor, it seems that the particle size of the material plays a key role. The smaller particle size for **Pt@COF** results in an improved accessibility to active centers over all the material and hence an increased reactivity. Moreover, it is worth to mention that pristine materials (in absence of Pt centers), although showed a limited activity for this reaction, are always much less effective than **Pt@COF** materials. Indeed, reaction conditions (time, solvents, etc) used in the present work only allow the observation of residual amounts of products under pristine COFs catalysis, while almost complete conversions are observed using **Pt@COF**. In addition, various experiments without irradiation or in presence of Ar atmosphere indicated that both light and molecular oxygen are indispensable for this oxidation process. Owing the better catalytic performance and the simplicity of the synthesis procedure for **Pt@COF**, the rest of experiments shown in this work were performed using this material.

Table 1: Screening of the sulfoxidation reaction [a].

Entry	Catalyst	Conversion (%) [b]
1	-	0
2	**Pt@COF**	88

3	**Pt@COF-Annealed**	75
4	**Pristine COF**	10
5	**Pristine COF-Annealed**	33

[a] Reactions were carried out with **3a** (0.3 mmol) and 2.4 mg of the corresponding catalyst in 2 mL of the indicated solvent under blue light irradiation and O_2 atmosphere (see Supporting Information for further details) after 7 hours. [b] Determined by ^{1}H NMR analysis of the crude mixture.

3.2.2. Recyclability, Stability and Leaching Experiments. A main advantage of performing catalytic transformations using **Pt@COF** arises from the different behaviour, of this material and complex **2** under analogous conditions. Interestingly, when the reaction was performed in the homogeneous system using complex **2,** adding the same number of equivalents of Platinum complex as those present in heterogeneous system, the reaction reached 60% yield after 2 h, but did not advance any further (Figure 3, red line), which represent a moderated TON (4875). However, the heterogeneous system has been proved to be much more robust. In fact, **Pt@COF** can perform several 8 hours catalytic runs that corresponded to 8125 TON each run at full conversion (Figure 3, black line). Therefore, although initial reaction rate is lower using **Pt@COF**, this material preserves the platinum centers to perform much more catalytic cycles than the homogeneous system, reaching approximately 25000 TON, much higher than 4875 TON for the homogeneously catalysed reaction. In addition, leaching processes have been discarded through several experiments: after one initial 8 h run, the reaction medium was filtrated, in which no detectable quantities of Pt were found using ICP-AES analysis. Furthermore, after the removal of the solid catalyst and the re-addition of 0.30

mmol of **3a**, no further reaction was observed for the next 16 hours (Figure 3, blue line). This result implies that there is no homogeneous catalytically active species in solution, and the observed catalytic activity is only attributed to the **Pt@COF**.
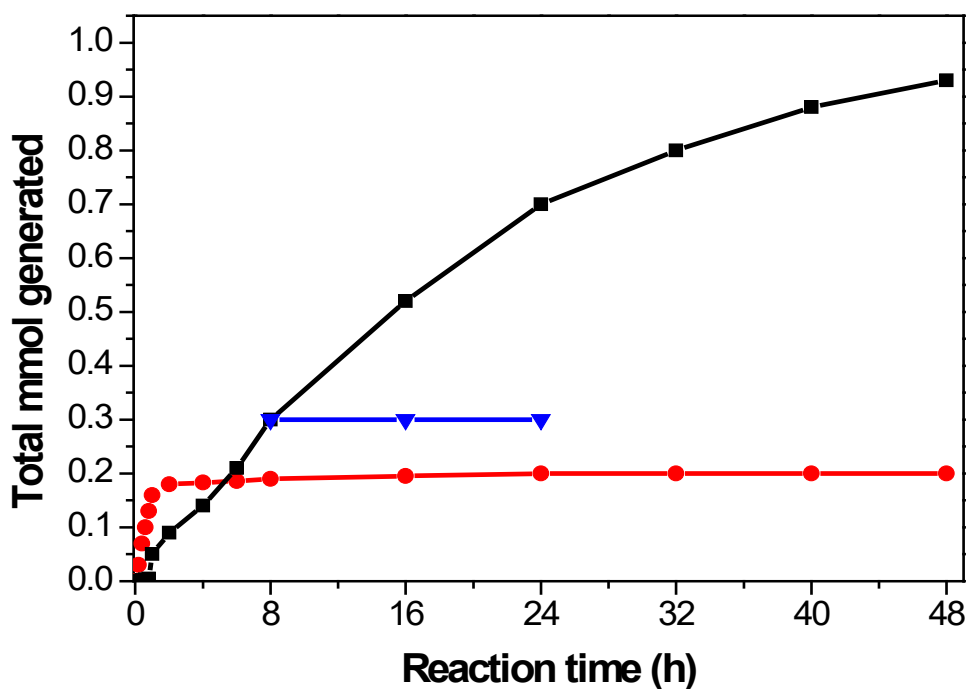

Figure 3: Catalytic evolution of the photooxidation of sulfide **3a** to sulfoxide **4a**. This essay was performed by the addition of 0.30 mmol of sulfide **3a** every 8 hours of reaction, under O_2 atmosphere (black squares for the **Pt@COF**-catalyzed reaction, and red circles for the homogeneous catalyzed reaction). The blue triangle line corresponds to the experiment carried out in order to test if leaching is produced: after a 8h catalytic run, reaction medium was filtrated and 0.3 mmol of **3a** were added, observing that the reaction did not advance further.

In order to better understand the differences in catalytic activity for the photocatalytic oxidation of methyl(*p*-tolyl)sulfide of the homogeneous and heterogeneous platinum-containing systems (Figure 3), X-ray synchrotron PDF experiments were performed to the catalyst after the reaction (see Figure 4). d-PDF

17

analyses on the molecular complex **2** in solution after catalysis, obtained by subtracting the PDF of the solvent to that of the Pt-complex in solution, showed the presence of a signal centred at ~2.6 Å associated with Pt-Pt correlations together with a signal at ~1.95 Å linked to Pt-N,O bond distances characteristic of the molecular complex (Figure 4, green line). This result suggests the significant aggregation of Pt during catalysis, which could be the cause of the loss of catalytic activity observed for the homogeneous system. However, due to the low concentration of Pt compound **2** used in this experiment (comparable to the platinum content on **Pt@COF**), observation of nanoparticles has not been possible by electron microscopy. d-PDF analyses of the heterogeneous **Pt@COF** system showed a significantly different structural scenario, with a signal centred at ~2.38 Å linked to Pt-Cl,S distances, as observed in Figure 2 for precatalysis-**Pt@COF**, and no evidence for the formation of Pt-Pt bonds (Figure 4, black line).
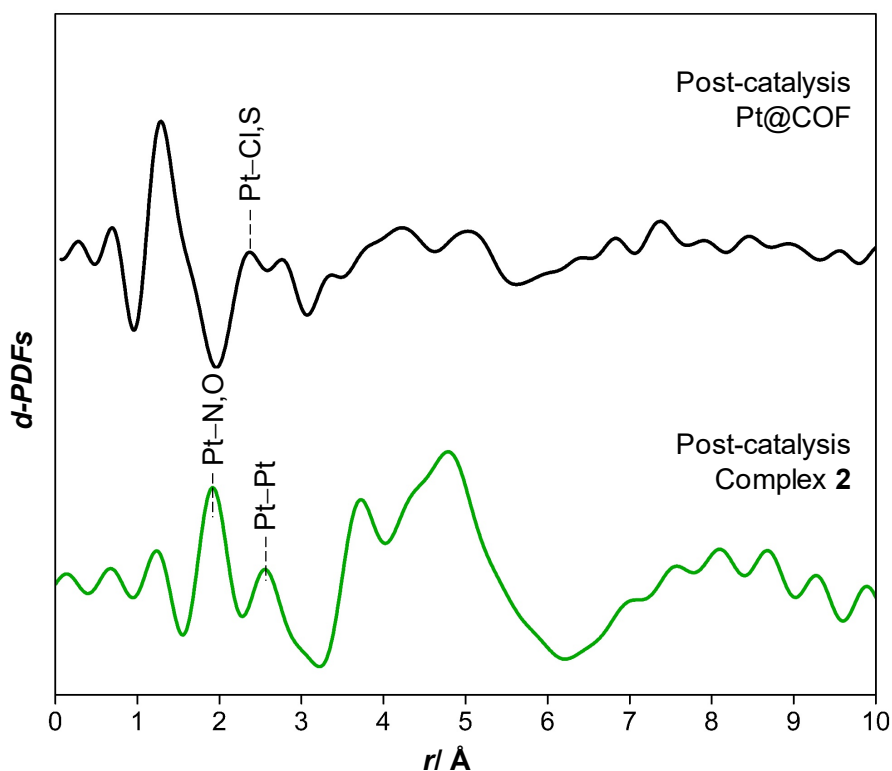
Figure 4: d-PDF data obtained for **Pt@COF** system as solid (black) and complex **1** in solution (green) after catalysis. The significant contribution at ~1.25 Å for **Pt@COF** is associated with the presence of guest organic molecules, including catalytic products, within the COF pores.

3.2.3. Mechanistic experiments. The effect of immobilization of platinum centers has been observed beyond their enhanced catalytic activity inside the organic framework. In addition, mechanistic data revealed some intriguing differences on the pathways followed by reactions catalysed by complex **2** or **Pt@COF**. Such observations have been made performing different indirect studies. Two different mechanisms[50] are possible for this reaction (Scheme 3): a) an energy transfer process, where singlet oxygen is the reactive oxygen species, or b) a photoredox process, where the transformation is mediated by superoxide radical anion and produces an intermediate radical cation sulfide species. Differentiation between these two mechanisms can be achieved by using selective additives that can act as quenchers or enhancers, indicating which is the predominant pathway and the reactive oxygen species. In particular, deuterated solvents accelerate the reaction *via* energy transfer.[51] On the other hand, 1,4-dimethoxybenzene (1,4-DMB) is able to act as a scavenger of radical-cation sulfide species, [50] that appear as a consequence of a photoredox mechanism. However, DABCO can react with singlet oxygen, inhibiting the energy transfer pathway.[50]

a) Energy transfer mechanism
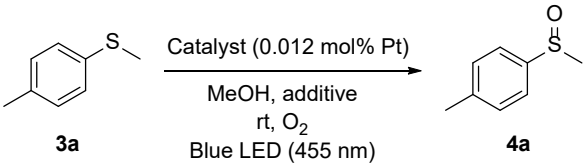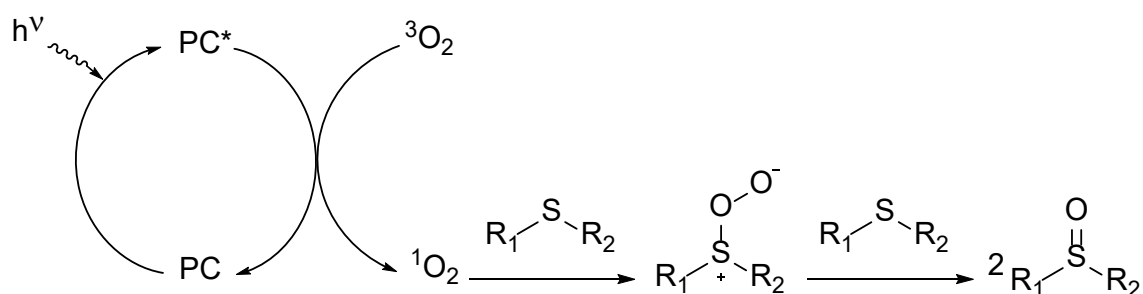

b) Electron transfer mechanism
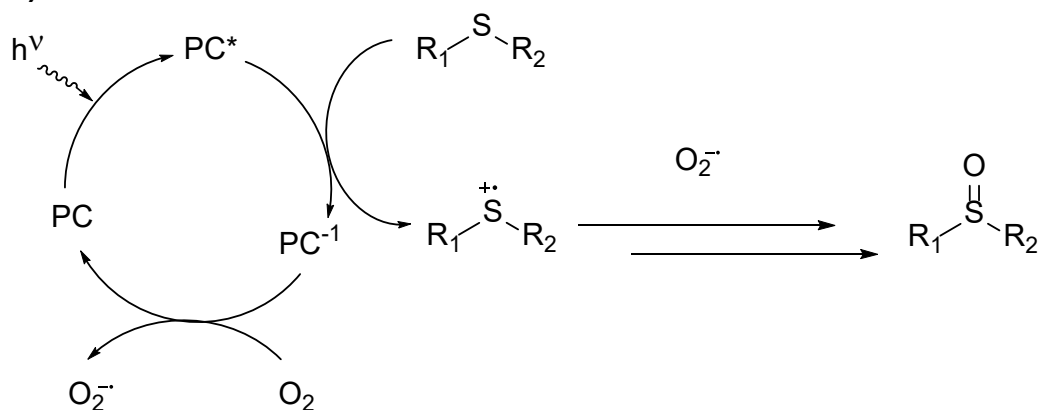
Scheme 3: The two possible mechanisms for the photooxidation of sulfoxides to sulfoxides under visible light conditions.

As previously reported for complex **1**,[34,46] complex **2** is only able to act as a photoredox catalyst, and its photocatalytic activity is only quenched by 1,4-DMB (Table 2, entry 8). However, when the reaction was performed using **Pt@COF** as catalyst, both energy transfer and photoredox pathways must be considered, because both scavengers decreased the reaction conversion, while using deuterated methanol increased the catalytic output. These results indicate that the covalent incorporation of complex **2** as defect into the structure of the imine-based layered COF completely modifies its photocatalytic activity, enabling not only photoredox transformations, but also energy transfer reactions. Such effect is probably the result of avoiding intermolecular Pt-Pt

20

encounters. In solution, interaction between platinum complexes should account for triplet annihilation, hampering energy transfer to oxygen molecule. However, being discarded such interactions on isolated Pt centres on **Pt@COF**, energy transfer appears as a possible pathway, expanding the applicability of the photocatalyst in other transformations.

Table 2: Experiments for the determination of the predominant mechanistic pathway in the photosulfoxidation reaction.[a]

Entry	Catalyst	Solvent	Additive (mol%)	Conversion (%)[b]
1	**Pt@COF**	CH_3OH	-	88
2	**Pt@COF**	CH_3OH	-	100
3	**Pt@COF**	CH_3OH	DABCO (50)	37
4	**Pt@COF**	CH_3OH	1,4-DMB	67
5	Complex **2**	CD_3OD	-	60
6	Complex **2**	CD_3OD	-	50
7	Complex **2**	CD_3OD	DABCO (50)	68
8	Complex **2**	CD_3OD	1,4-DMB	44

[a] Reactions were carried out with **3a** (0.3 mmol) in presence of the corresponding catalyst in 2 mL of solvent under blue light irradiation and O_2 atmosphere. [b] Determined by ^{1}H-NMR measured on the crude mixture after 8 h.

*3.2.4. Substrate scope of the sulfoxidation reaction under **Pt@COF** catalysis.* In order to evaluate the scope of the possible sulfoxidation reaction, the photooxidation of different sulfides using **Pt@COF** as catalyst was studied (Scheme 4). Sulfoxides with electron-donating groups at the aryl moiety (**4a-b**) were obtained in good yields and quite low reaction times, with high TON (around 7500). In the case of electron-withdrawing groups (**4c-d**), longer reaction times were required, but TON was maintained above 5000. In addition, the oxidation of sulfides with cyclopropyl (**4e**) and allyl (**4f**) substituents in the aliphatic moiety also worked with good yields and total selectivity, without detection of benzaldehyde or other subproducts. Moreover, dialkylsulfides (**4g-h**), even highly hindered, were also oxidized to the corresponding sulfoxides in shorter reaction times and excellent yields, reaching the highest TON (more than 8000). Finally, diphenylsulfoxide **4i** was obtained in moderated yield. It is well-known that this oxidation is difficult, and that this substrate is only oxidable when the reaction goes through a photoredox mechanism.[51] On the other hand, the 1-(methylsulfinyl)-4-nitrobenzene, **4d**, which is also transformed in this system, is only able to get oxidized when the reaction proceeds via singlet oxygen.[51] It is noteworthy that the substrates that proceed exclusively through one or another pathway are the less reactive. All these data taken together are in agreement with the mechanistic studies explained above: the **Pt@COF**, under these reaction conditions, is able to act both as an energy transfer and a photoredox catalyst. Remarkably, pristine COFs did not show any significant photocatalytic activity under these conditions, and consequently the results obtained are totally ascribed to the Pt complex.
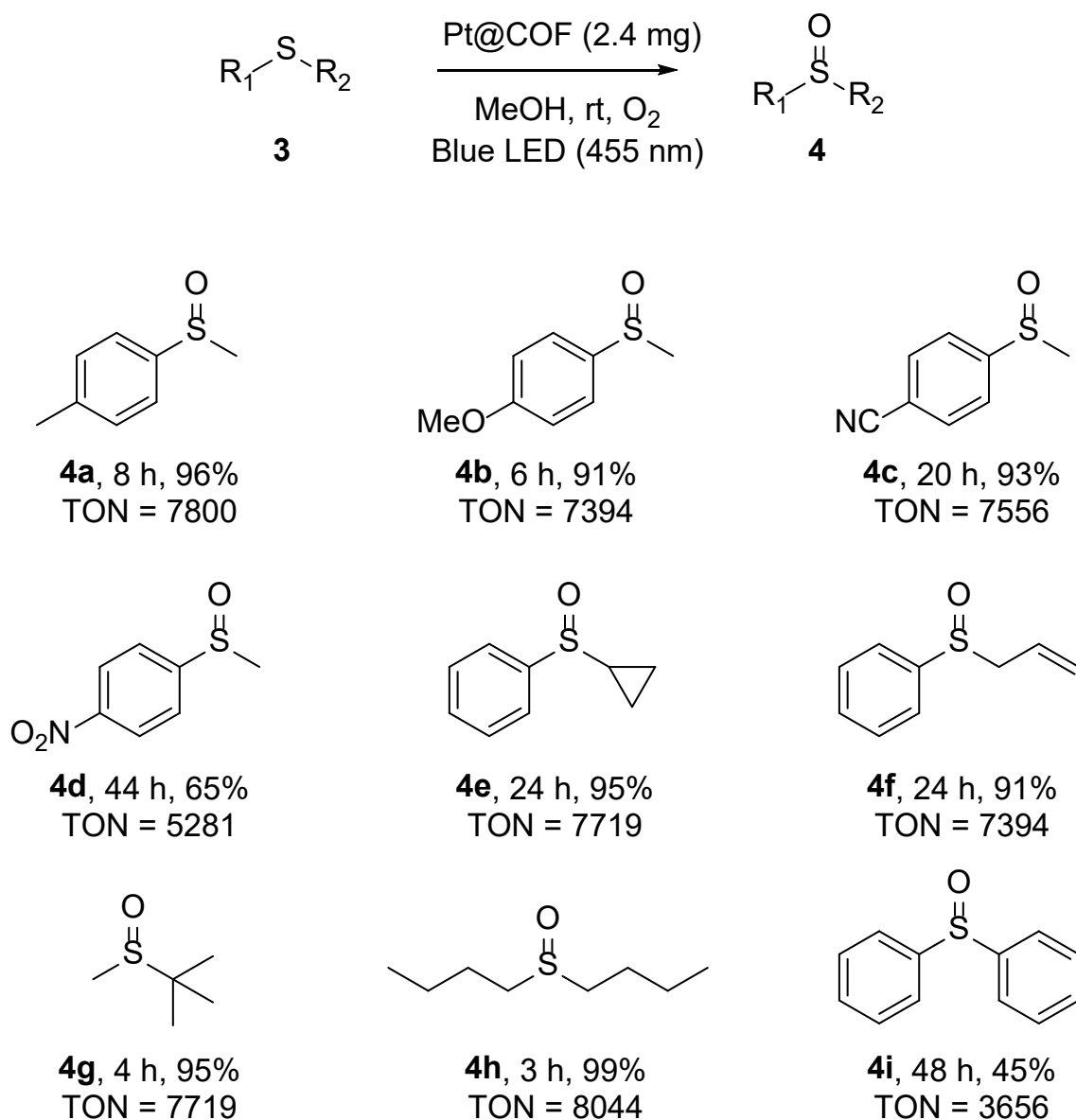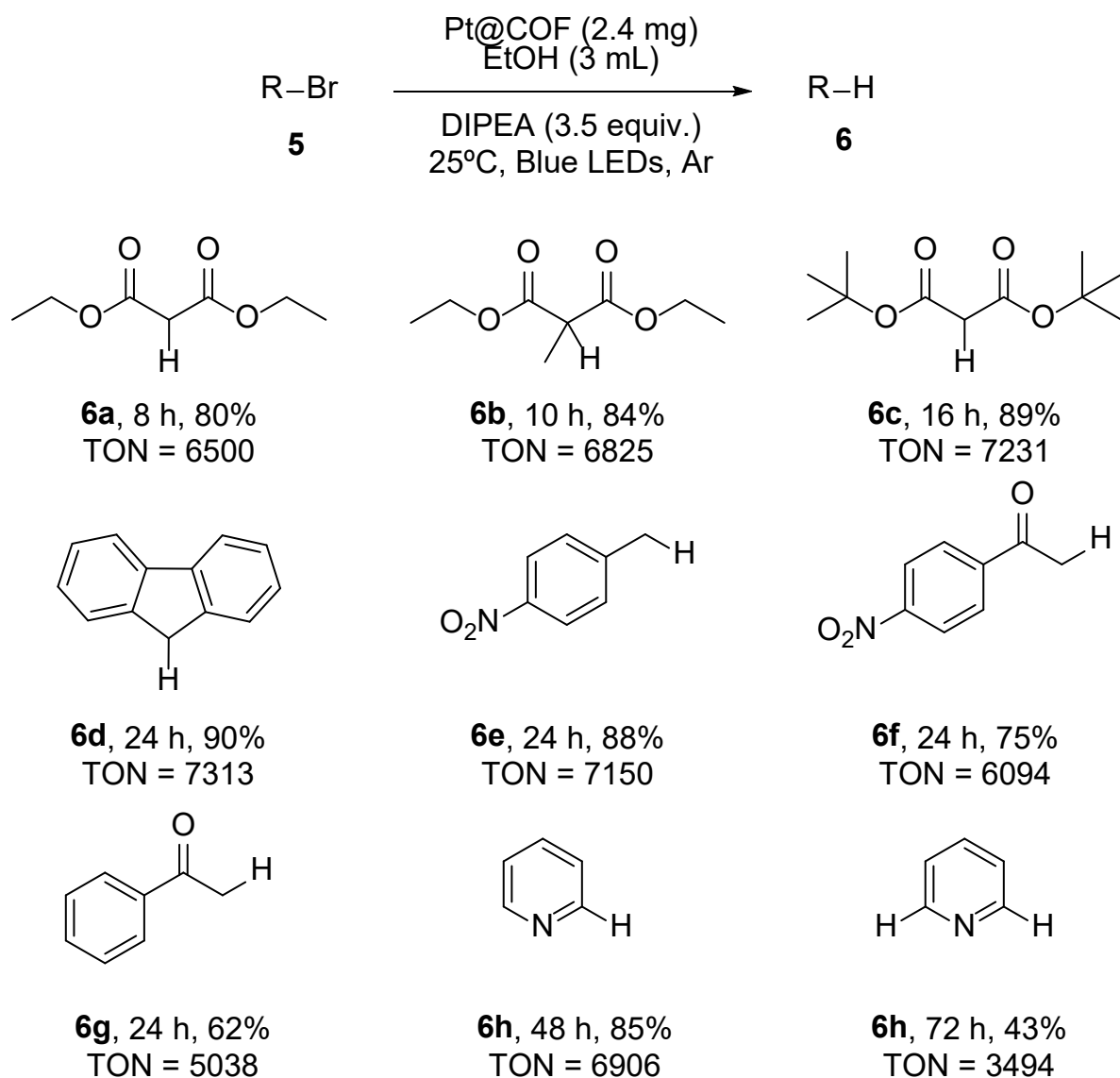
Scheme 4: Scope of the photosulfoxidation reaction using **Pt@COF** as catalyst. Reactions were carried out using **3** (0.3 mmol) and 2.4 mg of **Pt@COF** in 2 mL of MeOH under blue light irradiation and O_2 atmosphere. The yields were determined after the isolation of the product (see Supporting Information for further details).

3.3. Photocatalytic activity: hydrodebromination reaction.

Owing the double nature of the catalytic system (Energy Transfer – Photoredox), we extended the applicability of **Pt@COF** with the study of a reaction that proceeds through a purely photoredox mechanism: the photohydrodebromination of organic bromides.[46,52] This reaction has been scarcely explored under COF photocatalytic systems, being necessary the predesign of photoactive building blocks such as triphenylamines [53] or diazothiazoles.[54] However, undecorated imine-based COFs are not able to catalyze this reaction, since high reducing potentials are needed (< -1.2 V vs SCE).[55] In addition, only a few substrates with highly activated C-Br bonds have been efficiently reduced, such as phenacyl [54] or malonate bromides using non-ecofriendly solvents or high power light sources.[53] Moreover, this reaction is of environmental interest because brominated products are persistent pollutants, and its photodegradation is a promising way for its remediation.[55] Thus, we wondered if **Pt@COF**, which contains a powerful photoredox unit, would be capable of catalyzing this reaction under environmentally benign conditions. First of all, the photocatalytic hydrodebromination of the diethylbromomalonate, a readily reducible substrate, was carried out, using diisopropylethylamine (DIPEA) as a sacrificial electron donor (Scheme 5).[52] The results confirmed the high activity of the **Pt@COF** towards this reaction, with 80 % of yield after 8 h, using EtOH as green solvent. In addition, control experiments were performed in absence of catalyst or in presence of pristine layered COF, observing less than 5% of conversion, confirming that the observed photoredox activity is totally attributed to the immobilized Pt centers. This catalytic system demonstrates to be quite robust, being applied to more hindered bromomalonate derivatives **6b** and **6c**. In addition, benzylic bromides such as **6d** and **6e** were efficiently reduced under mild conditions and low reaction times. The reaction worked also for

phenacyl bromides (**6f**, **6g**). Finally, the more challenging aromatic substrates (Csp^2-Br) **6h** and dihalogen **6i** were readily reduced under longer reaction times. These results demonstrate the wide applicability of this material to different photocatalytic processes, presenting very high turnover numbers (up to 8000) and excellent photoredox properties.

$$R-Br \xrightarrow[\substack{DIPEA\ (3.5\ equiv.) \\ 25°C,\ Blue\ LEDs,\ Ar}]{\substack{Pt@COF\ (2.4\ mg) \\ EtOH\ (3\ mL)}} R-H$$

5   **6**

6a, 8 h, 80%
TON = 6500

6b, 10 h, 84%
TON = 6825

6c, 16 h, 89%
TON = 7231

6d, 24 h, 90%
TON = 7313

6e, 24 h, 88%
TON = 7150

6f, 24 h, 75%
TON = 6094

6g, 24 h, 62%
TON = 5038

6h, 48 h, 85%
TON = 6906

6h, 72 h, 43%
TON = 3494

Scheme 5: Scope of the photodebromination reaction under **Pt@COF** catalysis. The reaction was performed using 0.3 mmol of the corresponding brominated reagent in presence of 2.4 mg of **Pt@COF**, 3 mL of EtOH and 3.5 equivalents of DIPEA under blue light irradiation and Ar

atmosphere. The yields were obtained after isolation of the corresponding products (see Supporting Information for further details).

4. Conclusions

In conclusion, design of a new Pt(II)-hydroxyquinoline complex has allowed the covalent incorporation of photoactive Pt(II) centers into a 2D layered imine-based COF. For the first time, a metal center has been incorporated to a COF applying the monomer truncation strategy. This strategy has many advantages, such as: high versatility and simplicity, exhaustive control over the metal coordination environment and slight alteration of the material structure, allowing the obtention of heterogeneous photocatalyst with enhanced stability, recyclability and activity of the isolated catalytic centers. Despite the low content of Pt(II) (0.3% wt.) resulting from the reversibility of imine bonds, a great enhancement of the photocatalytic activity has been observed in comparison with molecular catalysts and pristine materials, being possible to reach up to 25000 TON for sulfoxidation processes. While complex **2** in solution can only proceed through a photoredox mechanism, **Pt@COF** is able to follow both energy transfer and photoredox pathways since is avoiding aggregation processes, which are responsible of the inactivation of homogeneous catalysts. Thus, not only a variety of organic sulfides have been selectively transformed into sulfoxides (energy transfer process), but also photohydrodebromination of bromo-derivatives (photoredox process), have been observed in excellent yields and very high turnover numbers.

Overall, the work presented herein extents the catalytic uses of functionalized COFs to a wide range of reactions mediated by metal centers with predetermined coordination environments, that can be easily attached to organic backbones through simple chemical transformations. The obtained results will contribute to the design of

catalytic heterogeneous systems with high activity, recyclability, selectivity and stability.

Competing financial interests

The authors declare no competing financial interests.

Apendix A

Supplementary Information

References

[1] A.P. Côté, A. I. Benin, N. W. Ockwig, M. O'Keeffe, A. J. Matzger, O. M. Yaghi, Porous , Crystalline , Covalent Organic Frameworks, Science 1166 (2007) 1166-1170. https://doi.org/10.1126/science.1120411.https://doi.org/10.1126/science.1120411.

[2] F.J. Uribe-Romo, J.R. Hunt, H. Furukawa, C. Klöck, M. O'Keeffe, O.M. Yaghi, A Crystalline Imine-Linked 3-D Porous Covalent Organic Framework, J. Am. Chem. Soc.

131 (2009) 4570–4571. https://doi.org/10.1021/ja8096256.

[3]   H. Furukawa, O.M. Yaghi, Storage of Hydrogen, Methane, and Carbon Dioxide in Highly Porous Covalent Organic Frameworks for Clean Energy Applications, J. Am. Chem. Soc. 131 (2009) 8875–8883. https://doi.org/10.1021/ja9015765.

[4]   C.J. Doonan, D.J. Tranchemontagne, T.G. Glover, J.R. Hunt, O.M. Yaghi, Exceptional ammonia uptake by a covalent organic framework, Nat. Chem. 2 (2010) 235–238. https://doi.org/10.1038/nchem.548.

[5]   S. Wan, J. Guo, J. Kim, H. Ihee, D. Jiang, A Photoconductive Covalent Organic Framework: Self-Condensed Arene Cubes Composed of Eclipsed 2D Polypyrene Sheets for Photocurrent Generation, Angew. Chemie Int. Ed. 48 (2009) 5439–5442. https://doi.org/10.1002/anie.200900881.

[6]   C.R. Mulzer, L. Shen, R.P. Bisbey, J.R. McKone, N. Zhang, H.D. Abruña, W.R. Dichtel, Superior Charge Storage and Power Density of a Conducting Polymer-Modified Covalent Organic Framework, ACS Cent. Sci. 2 (2016) 667–673. https://doi.org/10.1021/acscentsci.6b00220.

[7]   S. Chandra, D. Roy Chowdhury, M. Addicoat, T. Heine, A. Paul, R. Banerjee, Molecular Level Control of the Capacitance of Two-Dimensional Covalent Organic Frameworks: Role of Hydrogen Bonding in Energy Storage Materials, Chem. Mater. 29 (2017) 2074–2080. https://doi.org/10.1021/acs.chemmater.6b04178.

[8]   C.R. DeBlase, K.E. Silberstein, T.-T. Truong, H.D. Abruña, W.R. Dichtel, β-Ketoenamine-Linked Covalent Organic Frameworks Capable of Pseudocapacitive Energy Storage, J. Am. Chem. Soc. 135 (2013) 16821–16824. https://doi.org/10.1021/ja409421d.

[9]   Y. Zhang, J. Duan, D. Ma, P. Li, S. Li, H. Li, J. Zhou, X. Ma, X. Feng, B. Wang, Three-Dimensional Anionic Cyclodextrin-Based Covalent Organic Frameworks, Angew.

Chemie Int. Ed. 56 (2017) 16313–16317. https://doi.org/10.1002/anie.201710633.

[10] Y. Hu, N. Dunlap, S. Wan, S. Lu, S. Huang, I. Sellinger, M. Ortiz, Y. Jin, S. Lee, W. Zhang, Crystalline Lithium Imidazolate Covalent Organic Frameworks with High Li-Ion Conductivity, J. Am. Chem. Soc. 141 (2019) 7518–7525. https://doi.org/10.1021/jacs.9b02448.

[11] Q. Fang, J. Wang, S. Gu, R.B. Kaspar, Z. Zhuang, J. Zheng, H. Guo, S. Qiu, Y. Yan, 3D Porous Crystalline Polyimide Covalent Organic Frameworks for Drug Delivery, J. Am. Chem. Soc. 137 (2015) 8352–8355. https://doi.org/10.1021/jacs.5b04147.

[12] H. Ma, B. Liu, B. Li, L. Zhang, Y.-G. Li, H.-Q. Tan, H.-Y. Zang, G. Zhu, Cationic Covalent Organic Frameworks: A Simple Platform of Anionic Exchange for Porosity Tuning and Proton Conduction, J. Am. Chem. Soc. 138 (2016) 5897–5903. https://doi.org/10.1021/jacs.5b13490.

[13] Z. Meng, A. Aykanat, K.A. Mirica, Proton Conduction in 2D Aza-Fused Covalent Organic Frameworks, Chem. Mater. 31 (2019) 819–825. https://doi.org/10.1021/acs.chemmater.8b03897.

[14] H.S. Sasmal, H.B. Aiyappa, S.N. Bhange, S. Karak, A. Halder, S. Kurungot, R. Banerjee, Superprotonic Conductivity in Flexible Porous Covalent Organic Framework Membranes, Angew. Chemie Int. Ed. 57 (2018) 10894–10898. https://doi.org/10.1002/anie.201804753.

[15] S. Chandra, T. Kundu, K. Dey, M. Addicoat, T. Heine, R. Banerjee, Interplaying Intrinsic and Extrinsic Proton Conductivities in Covalent Organic Frameworks, Chem. Mater. 28 (2016) 1489–1494. https://doi.org/10.1021/acs.chemmater.5b04947.

[16] S. Wan, J. Guo, J. Kim, H. Ihee, D. Jiang, A Belt-Shaped, Blue Luminescent, and Semiconducting Covalent Organic Framework, Angew. Chemie Int. Ed. 47 (2008) 8826–8830. https://doi.org/10.1002/anie.200803826.

[17] G. Lin, H. Ding, D. Yuan, B. Wang, C. Wang, A Pyrene-Based, Fluorescent Three-Dimensional Covalent Organic Framework, J. Am. Chem. Soc. 138 (2016) 3302–3305. https://doi.org/10.1021/jacs.6b00652.

[18] J.W. Crowe, L.A. Baldwin, P.L. McGrier, Luminescent Covalent Organic Frameworks Containing a Homogeneous and Heterogeneous Distribution of Dehydrobenzoannulene Vertex Units, J. Am. Chem. Soc. 138 (2016) 10120–10123. https://doi.org/10.1021/jacs.6b06546.

[19] S.-Y. Ding, J. Gao, Q. Wang, Y. Zhang, W.-G. Song, C.-Y. Su, W. Wang, Construction of Covalent Organic Framework for Catalysis: Pd/COF-LZU1 in Suzuki–Miyaura Coupling Reaction, J. Am. Chem. Soc. 133 (2011) 19816–19822. https://doi.org/10.1021/ja206846p.

[20] J. Zhang, X. Han, X. Wu, Y. Liu, Y. Cui, Multivariate Chiral Covalent Organic Frameworks with Controlled Crystallinity and Stability for Asymmetric Catalysis, J. Am. Chem. Soc. 139 (2017) 8277–8285. https://doi.org/10.1021/jacs.7b03352.

[21] X. Han, Q. Xia, J. Huang, Y. Liu, C. Tan, Y. Cui, Chiral Covalent Organic Frameworks with High Chemical Stability for Heterogeneous Asymmetric Catalysis, J. Am. Chem. Soc. 139 (2017) 8693–8697. https://doi.org/10.1021/jacs.7b04008.

[22] X. Han, J. Zhang, J. Huang, X. Wu, D. Yuan, Y. Liu, Y. Cui, Chiral induction in covalent organic frameworks, Nat. Commun. 9 (2018) 1294. https://doi.org/10.1038/s41467-018-03689-9.

[23] H.B. Aiyappa, J. Thote, D.B. Shinde, R. Banerjee, S. Kurungot, Cobalt-Modified Covalent Organic Framework as a Robust Water Oxidation Electrocatalyst, Chem. Mater. 28 (2016) 4375–4379. https://doi.org/10.1021/acs.chemmater.6b01370.

[24] M. Lu, Q. Li, J. Liu, F.-M. Zhang, L. Zhang, J.-L. Wang, Z.-H. Kang, Y.-Q. Lan, Installing earth-abundant metal active centers to covalent organic frameworks for

efficient heterogeneous photocatalytic CO2 reduction, Appl. Catal. B Environ. 254 (2019) 624–633. https://doi.org/https://doi.org/10.1016/j.apcatb.2019.05.033.

[25]   L.-H. Li, X.-L. Feng, X.-H. Cui, Y.-X. Ma, S.-Y. Ding, W. Wang, Salen-Based Covalent Organic Framework, J. Am. Chem. Soc. 139 (2017) 6042–6045. https://doi.org/10.1021/jacs.7b01523.

[26]   H. Vardhan, G. Verma, S. Ramani, A. Nafady, A.M. Al-Enizi, Y. Pan, Z. Yang, H. Yang, S. Ma, Covalent Organic Framework Decorated with Vanadium as a New Platform for Prins Reaction and Sulfide Oxidation, ACS Appl. Mater. Interfaces. 11 (2019) 3070–3079. https://doi.org/10.1021/acsami.8b19352.

[27]   W. Leng, R. Ge, B. Dong, C. Wang, Y. Gao, Bimetallic docked covalent organic frameworks with high catalytic performance towards tandem reactions, RSC Adv. 6 (2016) 37403–37406. https://doi.org/10.1039/C6RA05304A.

[28]   E.M. Johnson, R. Haiges, S.C. Marinescu, Covalent-Organic Frameworks Composed of Rhenium Bipyridine and Metal Porphyrins: Designing Heterobimetallic Frameworks with Two Distinct Metal Sites, ACS Appl. Mater. Interfaces. 10 (2018) 37919–37927. https://doi.org/10.1021/acsami.8b07795.

[29]   W. Seo, D.L. White, A. Star, Fabrication of Holey Graphene: Catalytic Oxidation by Metalloporphyrin-Based Covalent Organic Framework Immobilized on Highly Ordered Pyrolytic Graphite, Chem. – A Eur. J. 23 (2017) 5652–5657. https://doi.org/10.1002/chem.201605488.

[30]   D.N. Bunck, W.R. Dichtel, Mixed Linker Strategies for Organic Framework Functionalization, Chem. – A Eur. J. 19 (2013) 818–827. https://doi.org/10.1002/chem.201203145.

[31]   D.N. Bunck, W.R. Dichtel, Internal Functionalization of Three-Dimensional Covalent Organic Frameworks, Angew. Chemie Int. Ed. 51 (2012) 1885–1889.

https://doi.org/10.1002/anie.201108462.

[32]   M. Calik, T. Sick, M. Dogru, M. Döblinger, S. Datz, H. Budde, A. Hartschuh, F. Auras, T. Bein, From Highly Crystalline to Outer Surface-Functionalized Covalent Organic Frameworks—A Modulation Approach, J. Am. Chem. Soc. 138 (2016) 1234–1239. https://doi.org/10.1021/jacs.5b10708.

[33]   Z. Li, Z.-W. Liu, Z. Li, T.-X. Wang, F. Zhao, X. Ding, W. Feng, B.-H. Han, Defective 2D Covalent Organic Frameworks for Postfunctionalization, Adv. Funct. Mater. 30 (2020) 1909267. https://doi.org/10.1002/adfm.201909267.

[34]   A. Casado-Sánchez, R. Gómez-Ballesteros, F. Tato, F.J. Soriano, G. Pascual-Coca, S. Cabrera, J. Alemán, Pt(ii) coordination complexes as visible light photocatalysts for the oxidation of sulfides using batch and flow processes, Chem. Commun. 52 (2016) 9137–9140. https://doi.org/10.1039/C6CC02452A.

[35]   J. Alemán, S. Cabrera, R. Mas-Ballesté, A. Jiménez-Almarza, A. López-Magano, L. Marzo, Imine-Based Covalent Organic Frameworks as Photocatalysts for Metal Free Oxidation Processes under Visible Light Conditions, ChemCatChem. 0 (2019). https://doi.org/10.1002/cctc.201901061.

[36]   S. Wild, D. McLagan, M. Schlabach, R. Bossi, D. Hawker, R. Cropp, C.K. King, J.S. Stark, J. Mondon, S.B. Nash, An Antarctic Research Station as a Source of Brominated and Perflutorinated Persistent Organic Pollutants to the Local Environment, Environ. Sci. Technol. 49 (2015) 103–112. https://doi.org/10.1021/es5048232.

[37]   R. Fernández-Ruiz, M.J. Redrejo, E.J. Friedrich, M. Ramos, T. Fernández, Evaluation of Bioaccumulation Kinetics of Gold Nanorods in Vital Mammalian Organs by Means of Total Reflection X-Ray Fluorescence Spectrometry, Anal. Chem. 86 (2014) 7383–7390. https://doi.org/10.1021/ac5006475.

[38]   R. Fernández-Ruiz, A. von Bohlen, E.J. Friedrich K, M.J. Redrejo, Analysis of coke

beverages by total-reflection X-ray fluorescence, Spectrochim. Acta Part B At. Spectrosc. 145 (2018) 99–106. https://doi.org/https://doi.org/10.1016/j.sab.2018.04.013.

[39]   M. Basham, J. Filik, M.T. Wharmby, P.C.Y. Chang, B. El Kassaby, M. Gerring, J. Aishima, K. Levik, B.C.A. Pulford, I. Sikharulidze, D. Sneddon, M. Webber, S.S. Dhesi, F. Maccherozzi, O. Svensson, S. Brockhauser, G. Náray, A.W. Ashton, {\it Data Analysis WorkbeNch} ({\it DAWN}), J. Synchrotron Radiat. 22 (2015) 853–858. https://doi.org/10.1107/S1600577515002283.

[40]   P. Juhás, T. Davis, C. ~L. Farrow, S. ~J. ~L. Billinge, {\it PDFgetX3}: a rapid and highly automatable program for processing powder diffraction data into total scattering pair distribution functions, J. Appl. Crystallogr. 46 (2013) 560–566. https://doi.org/10.1107/S0021889813005190.

[41]   B.J. Smith, A.C. Overholts, N. Hwang, W.R. Dichtel, Insight into the crystallization of amorphous imine-linked polymer networks to 2D covalent organic frameworks, Chem. Commun. 52 (2016) 3690–3693. https://doi.org/10.1039/C5CC10221A.

[42]   X. Jin, Z. Yang, T. Li, B. Wang, Y. Li, M. Yan, C. Liu, J. An, 8-hydroxyquinoline-5-carbaldehyde-(benzotriazol-1'-acetyl)hydrazone as a potential Mg2+ fluorescent chemosensor, J. Coord. Chem. 66 (2013) 300–305. https://doi.org/10.1080/00958972.2012.756102.

[43]   CCDC 1979009 contains the crystallographic data of Complex **2**. These data can be obtained free of charge from The Cambridge Crystallographic Data Centre via www.ccdc.cam.ac.uk/data_request/cif.

[44]   A. de la Peña Ruigómez, D. Rodríguez-San-Miguel, K.C. Stylianou, M. Cavallini, D. Gentili, F. Liscio, S. Milita, O.M. Roscioni, M.L. Ruiz-González, C. Carbonell, D. Maspoch, R. Mas-Ballesté, J.L. Segura, F. Zamora, Direct On-Surface Patterning of a Crystalline Laminar Covalent Organic Framework Synthesized at Room Temperature,

Chem. – A Eur. J. 21 (2015) 10666–10670. https://doi.org/10.1002/chem.201501692.

[45]   D. Rodríguez-San-Miguel, A. Abrishamkar, J.A.R. Navarro, R. Rodriguez-Trujillo, D.B. Amabilino, R. Mas-Ballesté, F. Zamora, J. Puigmartí-Luis, Crystalline fibres of a covalent organic framework through bottom-up microfluidic synthesis, Chem. Commun. 52 (2016) 9212–9215. https://doi.org/10.1039/C6CC04013F.

[46]   A. Casado-Sánchez, M. Uygur, D. González-Muñoz, F. Aguilar-Galindo, J.L. Nova-Fernández, J. Arranz-Plaza, S. Díaz-Tendero, S. Cabrera, O.G. Mancheño, J. Alemán, 8-Mercaptoquinoline as a Ligand for Enhancing the Photocatalytic Activity of Pt(II) Coordination Complexes: Reactions and Mechanistic Insights, J. Org. Chem. 84 (2019) 6437–6447. https://doi.org/10.1021/acs.joc.9b00520.

[47]   L. Liu, B. Zhang, X. Tan, D. Tan, X. Cheng, B. Han, J. Zhang, Improved photocatalytic performance of covalent organic frameworks by nanostructure construction, Chem. Commun. (2020). https://doi.org/10.1039/D0CC00761G.

[48]   Y. Meng, Y. Luo, J.-L. Shi, H. Ding, X. Lang, W. Chen, A. Zheng, J. Sun, C. Wang, 2D and 3D Porphyrinic Covalent Organic Frameworks: The Influence of Dimensionality on Functionality, Angew. Chemie Int. Ed. 59 (2020) 3624–3629. https://doi.org/10.1002/anie.201913091.

[49]   J. Luis-Barrerra, R. Cano, G. Imani-Shakibaei, J. Heras-Domingo, J. Pérez-Carvajal, I. Imaz, D. Maspoch, X. Solans-Monfort, J. Alemán, R. Mas-Ballesté, Switching acidic and basic catalysis through supramolecular functionalization in a porous 3D covalent imine-based material, Catal. Sci. Technol. 9 (2019) 6007–6014. https://doi.org/10.1039/C9CY01527B.

[50]   S.M. Bonesi, I. Manet, M. Freccero, M. Fagnoni, A. Albini, Photosensitized Oxidation of Sulfides: Discriminating between the Singlet-Oxygen Mechanism and Electron Transfer Involving Superoxide Anion or Molecular Oxygen, Chem. – A Eur. J. 12 (2006)

4844–4857. https://doi.org/10.1002/chem.200501144.

[51] J. Dad'ová, E. Svobodová, M. Sikorski, B. König, R. Cibulka, Photooxidation of Sulfides to Sulfoxides Mediated by Tetra-O-Acetylriboflavin and Visible Light, ChemCatChem. 4 (2012) 620–623. https://doi.org/10.1002/cctc.201100372.

[52] D. González-Muñoz, A. Casado-Sánchez, I. del Hierro, S. Gómez-Ruiz, S. Cabrera, J. Alemán, Size-selective mesoporous silica-based Pt(II) complex as efficient and reusable photocatalytic material, J. Catal. 373 (2019) 374–383. https://doi.org/https://doi.org/10.1016/j.jcat.2019.04.015.

[53] X. Kang, X. Wu, X. Han, C. Yuan, Y. Liu, Y. Cui, Rational synthesis of interpenetrated 3D covalent organic frameworks for asymmetric photocatalysis, Chem. Sci. 11 (2020) 1494–1502. https://doi.org/10.1039/C9SC04882K.

[54] Z. Li, Y. Zhi, P. Shao, H. Xia, G. Li, X. Feng, X. Chen, Z. Shi, X. Liu, Covalent organic framework as an efficient, metal-free, heterogeneous photocatalyst for organic transformations under visible light, Appl. Catal. B Environ. 245 (2019) 334–342. https://doi.org/https://doi.org/10.1016/j.apcatb.2018.12.065.

[55] J. Eriksson, N. Green, G. Marsh, Å. Bergman, Photochemical Decomposition of 15 Polybrominated Diphenyl Ether Congeners in Methanol/Water, Environ. Sci. Technol. 38 (2004) 3119–3125. https://doi.org/10.1021/es049830t.